J|A|C|S
ARTICLES
Published on Web 03/13/2007

Spectroscopic, Computational, and Kinetic Studies of the μ_4-Sulfide-Bridged Tetranuclear Cu_Z Cluster in N_2O Reductase: pH Effect on the Edge Ligand and Its Contribution to Reactivity

Somdatta Ghosh,[†] Serge I. Gorelsky,[†] Serena DeBeer George,[§] Jeannine M. Chan,[#] Inês Cabrito,[‡] David M. Dooley,[#] José J. G. Moura,[‡] Isabel Moura,[‡] and Edward I. Solomon*,[†]

Contribution from the Department of Chemistry, Stanford University, Stanford, California 94305, Stanford Synchrotron Radiation Laboratory, Stanford University, Stanford, California 94309, Department of Chemistry and Biochemistry, Montana State University, Bozeman, Montana 59717, and Departamento de Química, CQFB, Faculdade de Ciências e Tecnologia, Universidade Nova de Lisboa, 2825-114 Caparica, Portugal

Received November 10, 2006; E-mail: edward.solomon@stanford.edu

Abstract: A combination of spectroscopy and density functional theory (DFT) calculations has been used to evaluate the pH effect at the Cu_Z site in *Pseudomonas nautica* (Pn) nitrous oxide reductase (N_2OR) and *Achromobacter cycloclastes* (Ac) N_2OR and its relevance to catalysis. Absorption, magnetic circular dichroism, and electron paramagnetic resonance with sulfur K-edge X-ray absorption spectra of the enzymes at high and low pH show minor changes. However, resonance Raman (rR) spectroscopy of PnN_2OR at high pH shows that the 415 cm^{-1} Cu−S vibration (observed at low pH) shifts to higher frequency, loses intensity, and obtains a 9 cm^{-1} ^{18}O shift, implying significant Cu−O character, demonstrating the presence of a OH^- ligand at the Cu_ICu_{IV} edge. From DFT calculations, protonation of either the OH^- to H_2O or the μ_4-S^{2-} to μ_4-SH^- would produce large spectral changes which are not observed. Alternatively, DFT calculations including a lysine residue at an H-bonding distance from the Cu_ICu_{IV} edge ligand show that the position of the OH^- ligand depends on the protonation state of the lysine. This would change the coupling of the Cu−(OH) stretch with the Cu−S stretch, as observed in the rR spectrum. Thus, the observed pH effect (pK_a ~9.2) likely reflects protonation equilibrium of the lysine residue, which would both raise $E°$ and provide a proton for lowering the barrier for the N−O cleavage and for reduction of the $[Cu_4S(im)_7OH]^{2+}$ to the fully reduced $4Cu^I$ active form for turnover.

1. Introduction

N_2O is reduced by two electrons by the enzyme nitrous oxide reductase (N_2OR) in the last step of bacterial denitrification ($N_2O + 2H^+ + 2e^- \rightarrow N_2 + H_2O$).[1,2] N_2ORs from various organisms have been isolated aerobically and anaerobically since 1982; however, only recently have crystal structures of the enzyme (isolated under aerobic conditions) from three species, *Pseudomonas nautica* (Pn), *Paracoccus denitrificans* (Pd), and *Achromobacter cycloclastes* (Ac), been reported.[3−7] N_2OR is a homodimeric enzyme, with each subunit containing an electron-transferring Cu_A site in the C-terminal domain[8−11] and a catalytic Cu_Z site in the N-terminal domain.[12] The Cu_A-Cu_Z distance within a monomer is ~40 Å; however, the intermonomeric Cu_A-Cu_Z distance is ~10 Å,[3,6,13] which is within the range for efficient electron transfer (ET) in a protein, thus suggesting the requirement for dimerization. The Cu_A site in N_2OR has a structure closely similar to that of the Cu_A site in the cytochrome oxidases.[10,14−18] The Cu_Z site has a unique structural motif, consisting of a μ_4-sulfide-bridged tetranuclear Cu cluster. There

[†] Department of Chemistry, Stanford University.
[§] Stanford Synchrotron Radiation Laboratory, Stanford University.
[#] Montana State University.
[‡] Universidade Nova de Lisboa.

(1) Zumft, W. G. *Microbiol. Mol. Biol. Rev.* **1997**, *61*, 533.
(2) Zumft, W. G.; Kroneck, P. M. H. *Adv. Inorg. Biochem.* **1996**, *11*, 1993.
(3) Brown, K.; Tegoni, M.; Prudêncio, M.; Pereira, A. S.; Besson, S.; Moura, J. J.; Moura, I.; Cambillau, C. *Nat. Struct. Biol.* **2000**, *7*, 191.
(4) Brown, K.; Djinovic-Carugo, K.; Haltia, T.; Cabrito, I.; Saraste, M.; Moura, J. J. G.; Moura, I.; Tegoni, M.; Cambillau, C. *J. Biol. Chem.* **2000**, *275*, 41133.
(5) Prudencio, M.; Pereira, A. S.; Tavares, P.; Besson, S.; Cabrito, I.; Brown, K.; Samyn, B.; Devreese, B.; Van Beeumen, J.; Rusnak, F.; Fauque, G.; Moura, J. J. G.; Tegoni, M.; Cambillau, C.; Moura, I. *Biochemistry* **2000**, *39*, 3899.
(6) Haltia, T.; Brown, K.; Tegoni, M.; Cambillau, C.; Saraste, M.; Mattila, K.; Djinovic-Carugo, K. *Biochem. J.* **2003**, *369*, 77.
(7) Paraskevopoulos, K.; Antonyuk, S. V.; Sawers, R. G.; Eady, R. R.; Hasnain, S. S. *J. Mol. Biol.* **2006**, *362*, 55.
(8) Holm, R. H.; Kennepohl, P.; Solomon, E. I. *Chem. Rev.* **1996**, *96*, 2239.
(9) Ferguson-Miller, S.; Babcock, G. T. *Chem. Rev.* **1996**, *96*, 2889.
(10) Kroneck, P. M. H.; Antholine, W. E.; Riester, J.; Zumft, W. G. *FEBS Lett.* **1989**, *248*, 212.
(11) Kroneck, P. M. H.; Antholine, W. A.; Riester, J.; Zumft, W. G. *FEBS Lett.* **1988**, *242*, 70.
(12) Farrar, J. A.; Thomson, A. J.; Cheesman, M. R.; Dooley, D. M.; Zumft, W. G. *FEBS Lett.* **1991**, *294*, 11.
(13) Rosenzweig, A. C. *Nat. Struct. Biol.* **2000**, *7*, 169.
(14) Charnock, J. M.; Dreusch, A.; Korner, H.; Neese, F.; Nelson, J.; Kannt, A.; Michel, H.; Garner, C. D.; Kroneck, P. M. H.; Zumft, W. G. *Eur. J. Biochem.* **2000**, *267*, 1368.

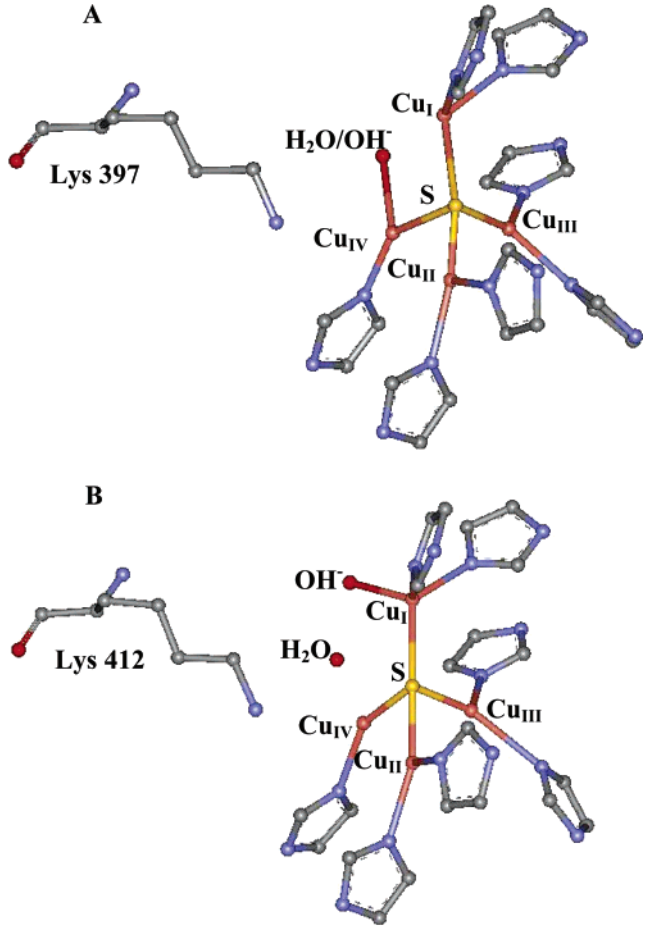

Figure 1. Crystal structures of (A) PnN$_2$OR (PDB code 1QNI)[3] and (B) AcN$_2$OR (PDB code 2IWF)[7] showing the Cu$_Z$ cluster, the O atoms of the edge ligands, and the lysine residue near the cluster. The protonation states of the edge ligands cannot be assigned from the X-ray data.

are seven histidine ligands coordinated to the Cu$_Z$ site (two ligated each to Cu$_{I,II,III}$ and one to Cu$_{IV}$) and a water-derived ligand at the Cu$_I$Cu$_{IV}$ edge, which is the proposed substrate binding site (Figure 1A).[3,6] The crystal structure of AcN$_2$OR shows the presence of two oxygen atoms (ascribed to a OH$^-$ near Cu$_I$ and a H$_2$O near Cu$_{IV}$) at the substrate binding site (Figure 1B).[7,19]

N$_2$OR can be isolated in different redox states, depending on whether it is isolated aerobically or anaerobically, and much spectroscopic data on the Cu$_Z$ site have been published.[5,12,20−24] The aerobically isolated form of N$_2$OR studied by crystallography has been spectroscopically characterized and found to contain Cu$_Z$ in the 1Cu^{II}/3Cu^I redox state with a total spin of $^1/_2$.[25,26] Electron paramagnetic resonance (EPR) data and density functional theory (DFT) calculations show that the unpaired electron is delocalized between two or more Cu atoms and the μ_4-sulfide, indicating that Cu$_Z$ is a mixed-valence system.[27−29]

Recently, we have shown that the Cu$_Z$ cluster can be further reduced to the 4Cu^I form on prolonged incubation with reduced methyl-viologen (MV).[30] This 4Cu^I form of the cluster has been determined to be the catalytically active form involved in N$_2$O reduction, which has been supported by Dooley and coworkers.[31] DFT calculations indicate that the energy of binding N$_2$O to the 4Cu^I form of Cu$_Z$ is higher than that for the resting 1Cu^{II}/3Cu^I redox form due to enhanced back-donation from the fully reduced Cu$_Z$ cluster to the bent μ-1,3-bridged N$_2$O ligand. Recently, a detailed mechanism for N$_2$O reduction by the Cu$_Z$ site has been developed using DFT calculations coupled to these data.[32] These calculations suggest the possibility of a direct cleavage of the N−O bond in the Cu$_Z$−N$_2$O complex because of the low reaction barrier (18 kcal mol^{-1}), associated with stabilization of the transition state by a strong Cu$_{IV}^{2+}$−O$^-$ bond. The two copper atoms (Cu$_I$ and Cu$_{IV}$) at the ligand binding site of the cluster play a crucial role in the reaction, as these Cu atoms are directly involved in N$_2$O binding, bending the ligand to a configuration (N−N−O angle = ∼139°) that resembles the transition state and contributing the two electrons needed for N$_2$O reduction. The other atoms of the Cu$_Z$ cluster maintain the needed structural motif and make Cu$_I$ and Cu$_{IV}$ better electron donors to enhance the back-bonding required for N$_2$O activation.[32]

Despite crystallographic, spectroscopic, and computational studies on the Cu$_Z$ site, the nature of the Cu$_I$Cu$_{IV}$ edge ligand still remains ambiguous. In addition, the protonation of the μ_4-sulfide of the cluster has not been experimentally evaluated. Past studies have defined the pH dependence of N$_2$OR activity, with an optimum activity in the range of pH 8−9.5, depending on the enzyme source.[33−35] This could be attributed to a protonation equilibrium of the Cu$_I$Cu$_{IV}$ edge ligand, or a nearby residue involved in the rate-determining step, or the μ_4-sulfide, or all three.

In this study we have used absorption, magnetic circular dichroism (MCD), resonance Raman (rR), EPR, and S K-edge spectroscopy to evaluate the effect of pH on the geometric and electronic structures of the Cu$_Z$ clusters of PnN$_2$OR and AcN$_2$-

(15) Kelly, M.; Lappalainen, P.; Talbo, G.; Haltia, T.; van der Oost, J.; Saraste, M. *J. Biol. Chem.* **1993**, *268*, 16781.
(16) Scott, R. A; Zumft, W. G; Coyle, C. L; Dooley, D. M. *Proc. Natl. Acad. Sci U.S.A.* **1989**, *86*, 4082.
(17) Kroneck, P. M. H.; Antholine, W. E.; Kastrau, D. H. W.; Buse, G.; Steffens, G. C. M.; Zumft, W. G. *FEBS Lett.* **1990**, *268*, 274.
(18) Antholine, W. E.; Kastrau, D. H. W.; Steffens, G. C. M.; Buse, G.; Zumft, W. G.; Kroneck, P. M. H. *Eur. J. Biochem.* **1992**, *209*, 875.
(19) The X-ray structures of the enzymes were obtained using the crystals from the solutions of pH 7.6−8, which should correspond to the low-pH forms of the Cu$_Z$ species of the current study.
(20) Alvarez, M. L.; Ai, J. Y.; Zumft, W.; Sanders-Loehr, J.; Dooley, D. M. *J. Am. Chem. Soc.* **2001**, *123*, 576.
(21) Farrar, J. A.; Zumft, W. G.; Thomson, A. J. *Proc. Natl. Acad. Sci. U.S.A.* **1998**, *95*, 9891.
(22) Rasmussen, T.; Berks, B. C.; Sanders-Loehr, J.; Dooley, D. M.; Zumft, W. G.; Thomson, A. J. *Biochemistry* **2000**, *39*, 12753.
(23) Dooley, D. M.; McGuirl, M. A.; Rosenzweig, A. C.; Landin, J. A.; Scott, R. A.; Zumft, W. G.; Devlin, F.; Stephens, P. J. *Inorg. Chem.* **1991**, *30*, 3006.
(24) Dooley, D. M.; Moog, R. S.; Zumft, W. G. *J. Am. Chem. Soc.* **1987**, *109*, 6730.
(25) Chen, P.; DeBeer George, S.; Cabrito, I.; Antholine, W. E.; Moura, J. J. G.; Moura, I.; Hedman, B.; Hodgson, K. O.; Solomon, E. I. *J. Am. Chem. Soc.* **2002**, *124*, 744.
(26) Chen, P.; Cabrito, I.; Moura, J. J. G.; Moura, I.; Solomon, E. I. *J. Am. Chem. Soc.* **2002**, *124*, 10497.
(27) Chen, P.; Gorelsky, S. I.; Ghosh, S.; Solomon, E. I. *Angew. Chem., Intl. Ed.* **2004**, *43*, 4132.
(28) Oganesyan, V. S.; Rasmussen, T.; Fairhurst, S.; Thomson, A. J. *Dalton Trans.* **2004**, 996.
(29) Rasmussen, T.; Berks, B. C.; Butt, J. N.; Thomson, A. J. *Biochem. J.* **2002**, 807.
(30) Ghosh, S.; Gorelsky, S. I.; Chen, P.; Cabrito, I.; Moura, J. J. G.; Moura, I.; Solomon, E. I. *J. Am. Chem. Soc.* **2003**, *125*, 15708.
(31) Chan, J. M.; Bollinger, J. A.; Grewell, C. L.; Dooley, D. M. *J. Am. Chem. Soc.* **2004**, *126*, 3030.
(32) Gorelsky, S. I.; Ghosh, S.; Solomon, E. I. *J. Am. Chem. Soc.* **2006**, *128*, 278.
(33) Coyle, C. L.; Zumft, W. G.; Kroneck, P. M. H.; Koerner, H.; Jakob, W. *Eur. J. Biochem.* **1985**, *153*, 459.
(34) Berks, B. C.; Baratta, D.; Richardson, D. J.; Ferguson, S. J. *Eur. J. Biochem.* **1993**, *212*, 467.
(35) Yamaguchi, K.; Kawamura, A.; Ogawa, H.; Suzuki, S. *J. Biochem.* (*Tokyo, Japan)* **2003**, *134*, 853.

OR. A large change in the rR spectrum was observed with a pK_a of ~9.2. Spectroscopic studies were then performed at a lower pH (6−7) and a higher pH (10.5) to study the pure species present as an equal mixture at this pK_a.[36] We then used DFT calculations to analyze these results and elucidate the nature of the Cu_ICu_{IV} edge ligand. We have also computationally evaluated the various protonation states of the edge ligand, the μ_4-sulfide, and a nearby lysine residue. The pH dependence of the kinetics of the reduction of the Cu_Z cluster has been determined to gain insight into the contributions of the protonation equilibrium toward reactivity.

2. Experimental Methods

2.1. Materials. All reagents were of the highest grade commercially available and were used without further purification. PnN_2OR was aerobically isolated and purified in Tris buffer, as previously reported,[4,5] and details of AcN_2OR expression and anaerobic purification will be reported elsewhere. The enzymes were exchanged to deuterated buffers at different pHs for spectroscopic and kinetic studies. Enzymatic activities and copper and sulfur contents were characterized as previously reported.[4,5,30,31] Excess dithionite solution was added to reduce the Cu_A center to make it spectroscopically silent (inferred from EPR and absorption spectra), while the oxidation state of the Cu_Z site remained unchanged. Excess ascorbate solution with prolonged incubation was used to reduce the Cu_A site (inferred from EPR and absorption spectra) of the S K-edge X-ray absorption spectroscopy (XAS) samples to avoid interfering sulfur signals from dithionite. Specific activities of the enzymes were measured by pre-incubating the enzyme with excess dithionite-reduced MV.[30,31] Glassed samples for MCD experiments were prepared by adding 50% (v/v) buffer/glycerol-$(OD)_3$. Addition of glycerol had no effect on the CD/EPR spectra of the enzymes. Epsilon values (per dimer, containing two Cu_Z centers) reported have been estimated by EPR spin quantification. $H_2{}^{18}O$ (95−97% purity) was purchased from Cambridge Isotopes. Approximate concentration of samples used for spectroscopy was 0.5 mM.

2.2. Spectroscopic Studies. Low-temperature absorption measurements were performed on a double-beam spectrophotometer (Cary 500) using a liquid helium cryostat (Janis Research Super Vari-Temp). MCD data were collected on CD spectro-polarimeters (JASCO J810 with an S20 PM tube for the UV/vis region, and J200 with an InSb detector for the near-IR region) with sample compartments modified to accommodate magnetocryostats (Oxford Instruments, SM4-7T). EPR spectra were obtained using a Bruker EMX spectrometer, an ER 041 XG microwave bridge, and an ER 4102ST cavity. All X-band samples were run at 77 K in a liquid nitrogen finger dewar. A Cu standard (1.0 mM $CuSO_4 \cdot 5H_2O$ with 2 mM HCl and 2 M $NaClO_4$) was used for spin quantitation of the EPR spectra. Q-band spectra were obtained at 77 K using an ER 051 QR microwave bridge, an ER 5106QT resonator, and an Oxford continuous-flow CF935 cryostat. EPR spectra were baseline-corrected and simulated using XSophe (Bruker). For a given enzyme, X- and Q-band spectra were simultaneously fit in order to constrain the simulation parameters (g values were obtained from Q-band and hyperfine constants from X-band EPR). rR spectra were obtained using a series of lines from Kr^+ (Coherent 190CK) and Ar^+ (Coherent Sabre 25/7) ion lasers with incident power ranging from 10 to 50 mW in an ~135° backscattering configuration. Dye (Rhodamine 6G, Coherent 599) and Ti-sapphire (Coherent 890) lasers were used for other spectral regions. Scattered light was dispersed through a triple monochromator (Spex 1877 CP, with 1200, 1800, and 2400 grooves mm^{-1} gratings) and detected with a back-illuminated CCD camera (Princeton Instruments ST-135). Samples contained in NMR tubes were immersed in a liquid nitrogen finger dewar. Raman peak intensities were referenced to the ice peak at ~230 cm^{-1} for rR excitation profiles. Background spectra of charcoal in the same NMR tube were subtracted to remove the quartz scattering. Sulfur K-edge data were measured at the Stanford Synchrotron Radiation Laboratory under ring conditions of 3.0 GeV and 60−100 mA, using the 54-pole wiggler beam line 6-2 in high magnetic field mode of 10 kG with a Ni-coated harmonic rejection mirror and fully tuned Si(111) double-crystal monochromator. Details of the optimization of this setup for low-energy studies have been described previously.[37] Protein samples were loaded in an inert atmosphere glove box and were immediately transferred to a helium-purged sample space. Protein solutions were loaded via syringe into a Pt-coated Al block sample holder with a 6.35-μm-thick polypropylene window. S K-edge measurements were made at ~4 °C. The data were measured as fluorescence excitation spectra utilizing an ionization chamber as a fluorescence detector. The energy was calibrated using the S K-edge spectrum of $Na_2S_2O_3 \cdot 5H_2O$, run at intervals between sample scans. The maximum of the first pre-edge feature in the spectrum was fixed at 2472.02 eV. A step size of 0.08 eV was used over the edge region. Data were averaged, and a smooth background was removed from all spectra by fitting a polynomial to the pre-edge region and subtracting this polynomial from the entire spectrum. Normalization of the data was accomplished by fitting a flattened polynomial or straight line to the post-edge region and normalizing the edge jump to 1.0 at 2490 eV.

2.3. Kinetic Studies. PnN_2OR (0.5 mM) was buffer-exchanged to different pHs and incubated with a 500-fold excess of dithionite-reduced MV (250 mM). The loss of one-hole Cu_Z EPR signal intensity was then measured at different time intervals, normalized with respect to the spectrum of the dithionite-reduced sample collected at time = 0 min. The temperature for the kinetic measurements was 25 °C.

2.4. Computational Details. The Cu_Z active site has been modeled as previously described (Figure S1A,B). In order to probe the influence of the deprotonated/proponated lysine residue near the Cu_ICu_{IV} edge of the Cu_Z cluster, the molecular model in this work has been extended to include the lysine and phenylalanine residues (Figure S1C,D). The total number of atoms in these extended simulations was 127−129 (64 heavy atoms). The C_β and C_γ atoms of the lysine residue and the carbon atoms of the phenylalanine residue were kept fixed during the geometry optimizations. The 6-311++G** basis set was used for the atoms of the active center (Cu_4SN_7), the edge ligands, and the lysine $-NH_2$/NH_3^+ group, and the 6-31G* basis set was used for the other atoms. The 6-311++G** basis set is necessary for accurate modeling of the Cu_Z cluster through the minimization of basis set superposition error effects for both energy and geometry-optimization results.

DFT calculations have been performed using the Gaussian 03 program.[38] Spin-unrestricted DFT was employed to model the open-shell species. Optimized molecular geometries were calculated using the hybrid B3LYP exchange-correlation functional[39−41] with tight SCF convergence criteria (10^{-8} au). Wave function stability calculations were performed to confirm that the calculated wave functions corresponded to the ground state. Frequency calculations were performed to ensure that the stationary points were minima and to calculate vibrational spectra. Time-dependent DFT (TD-DFT) was used to calculate the energies and intensities of the 40 lowest-energy, spin-allowed electronic transitions. The calculated absorption energies and intensities were transformed with the SWizard program[42] into simulated spectra as described before,[43] using Gaussians with half-widths ($\Delta_{1/2}$) of 3000 cm^{-1}.

(36) Studies at a pH range of 8.5−9 (where enzyme activity is optimum) would lead to a 50:50 equilibrium mixture of the low- and high-pH forms of the Cu_Z species.

(37) Hedman, B.; Frank, P.; Gheller, S. F.; Roe, A. L.; Newton, W. E.; Hodgson, K. O. *J. Am. Chem. Soc.* **1988**, *110*, 3798.
(38) Frisch, M. J.; et al. *Gaussian 03*, Revision C.02; Gaussian, Inc.: Wallingford, CT, 2004.
(39) Perdew, J. P. *Phys. Rev. B* **1986**, *33*, 8822.
(40) Becke, A. D. *Phys. Rev. A* **1988**, *38*, 3098.
(41) Becke, A. D. *J. Chem. Phys.* **1993**, *98*, 5648.
(42) Gorelsky, S. I. *SWizard;* Department of Chemistry, York University: Toronto, ON, 1999 (http://www.sg-chem.net).
(43) Gorelsky, S. I.; Lever, A. B. P. *J. Organomet. Chem.* **2001**, *635*, 187.

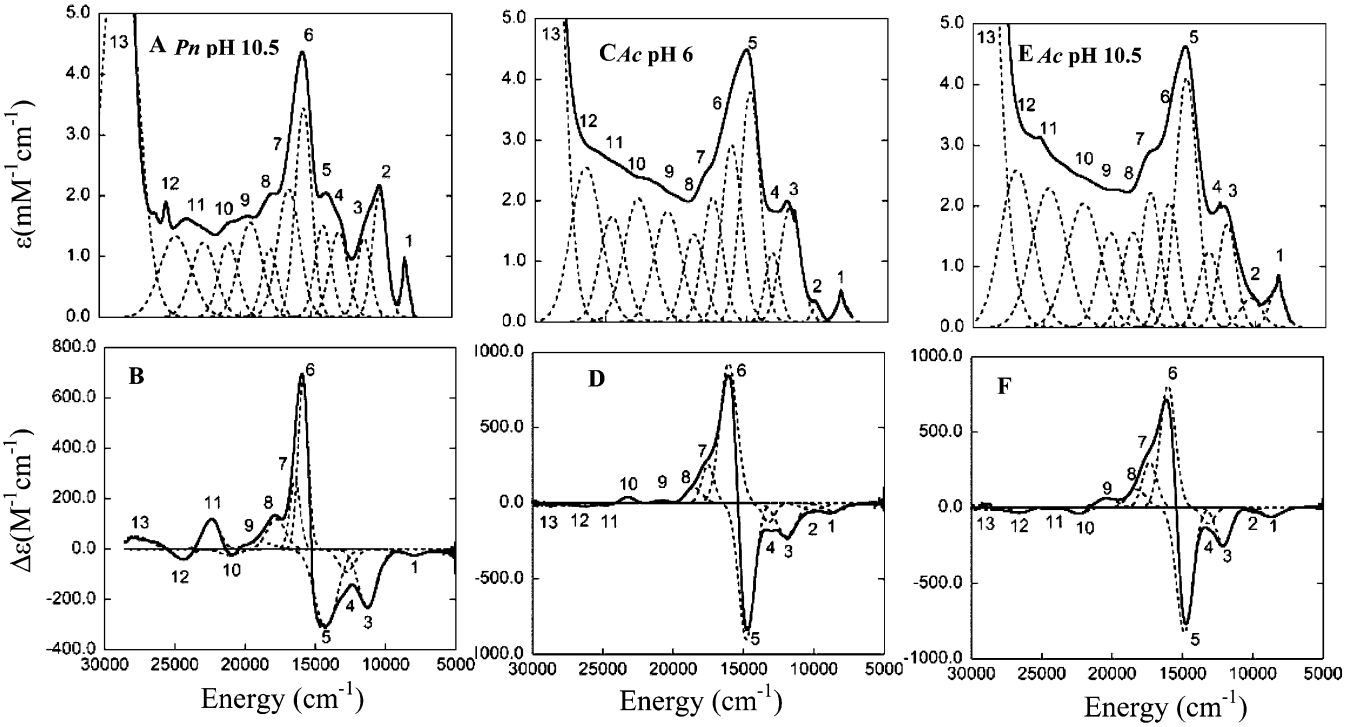

Figure 2. Optical spectra of dithionite-reduced Cu_Z: (A) PnN_2OR, pH 10.5, 10 K absorption; (B) PnN_2OR, pH 10.5, 5 K, 7 T MCD; (C) AcN_2OR, pH 6, 10 K, absorption; (D) AcN_2OR, pH 6, 5 K, 7 T MCD; (E) AcN_2OR, pH 10.5, 10K absorption; and (F) AcN_2OR, pH 10.5, 5 K, 7 T MCD.

Atomic charges and spin densities were calculated using the natural population analysis (NPA)[44] as implemented in Gaussian 03. The Mayer bond orders (BOs) were obtained to analyze covalent contributions to chemical bonding between the molecular fragments.[45,46] The bond order contributions from α- and β-spin molecular orbitals (BOP^{α} and BOP^{β}, respectively) and atomic indices were calculated using the AOMix-L program[47] and used in the analysis of chemical bonding. These calculations (the bond order analysis and the calculation of atomic valence indices) were performed using TZVP[48] on the Cu_4S cluster, the edge ligands, and the lysine $-NH_2/NH_3^+$ group and 6-31G* on the other atoms.

3. Results and Analysis

3.1. Spectroscopy. 3.1.1. Absorption and MCD. The absorption and MCD spectra of the dithionite-reduced (i.e., Cu_A reduced and Cu_Z in the $1Cu^{II}/3Cu^{I}$ redox state) samples of PnN_2OR (pH 10.5) and AcN_2OR at pH 6 and 10.5 are presented in Figure 2. Both the absorption and MCD spectra have intense S−Cu charge-transfer (CT) bands at around 15 600 cm^{-1} (640 nm), giving Cu_Z its characteristic blue color. The MCD spectrum of these enzymes also has an intense derivative-shaped pseudo-A-type signal in the S−Cu CT region. The absorption and MCD spectra of Cu_A-reduced PnN_2OR at pH 7, reported previously[26] (Figure S4A,B, adapted from ref 26), have been simultaneously fit with 13 bands (Table 1). Bands 1, 3, 4, and 8 were assigned as Cu d−d transitions, band 2 as an inter-valence transition (IT), bands 5−7 as the S−Cu CT transitions, and bands 9−13 as the histidine-to-Cu CT transitions. The orientations of the non-primed and primed axes systems in Table 1 are shown in Figure S2, and the details of these assignments are presented in ref 26.

Table 1. Gaussian-Resolved Peak Positions for Absorption and MCD Spectra of PnN_2OR and AcN_2OR at High and Low pHs[a]

		ν_{max} (cm^{-1})			
		PnN_2OR		AcN_2OR	
band	assignment	pH 7	pH 10.5	pH 6	pH 10.5
1	Cu d_{z^2}	8 015	8 100	8 400	8 500
2	IT	10 000	10 100	10 100	10 200
3	Cu d_{xz}	11 140	11 250	11 950	12 050
4	Cu d_{yz}	12 900	12 900	13 200	13 225
5	S $p_{z'}$	14 300	14 200	14 768	14 900
6	S $p_{x'}$	15 675	15 700	16 070	16 070
7	S $p_{y'}$	16 520	16 500	17 480	17 380
8	Cu d_{xy}	17 980	17 820	18 600	18 450
9	Π_1	19 775	19 136	20 700	20 300
10	Π_1	20 985	20 980	22 950	22 261
11	Π_1	22 270	22 500	24 600	24 600
12	Π_1	24 030	24 500	26 300	26 700
13	Π_2	28 055	28 150	28 600	29 600

[a] The assignments are according to ref 26. The coordinate system is given in Figure S2.

The absorption and MCD spectra of the anaerobically isolated AcN_2OR reduced with dithionite (i.e., Cu_A reduced and Cu_Z in the $1Cu^{II}/3Cu^{I}$ form) at pH 6 are shown in Figure 2C,D. Simultaneous Gaussian fitting of the absorption and MCD spectra also give 13 bands, which can be assigned in parallel with those of PnN_2OR. The spectra of PnN_2OR and AcN_2OR look very similar but have some quantitative differences. In general, all the bands in AcN_2OR are blue-shifted (Table 1). There is also intensity redistribution in the S−Cu CT bands in the absorption spectra of the two enzymes (Figures S4A and 2C), with band 5 being the most intense in AcN_2OR compared to band 6 in PnN_2OR. This is also reflected in the rR profiles (*vide infra*) and MCD spectra (Figures S4B and 2D), where

(44) Reed, A. E.; Weinstock, R. B.; Weinhold, F. *J. Chem. Phys.* **1985**, *83*, 735.
(45) Gorelsky, S. I.; Basumallick, L.; Vura-Weis, J.; Sarangi, R.; Hedman, B.; Hodgson, K. O.; Fujisawa, K.; Solomon, E. I. *Inorg. Chem.* **2005**, *44*, 4947.
(46) Mayer, I. *Chem. Phys. Lett.* **1983**, *97*, 270.
(47) Gorelsky, S. I. *AOMix Software Package*; Department of Chemistry, York University: Toronto, ON, 1998 (http://www.sg-chem.net).
(48) Schafer, A.; Huber, C.; Ahlrichs, R. *J. Chem. Phys.* **1994**, *100*, 5829.

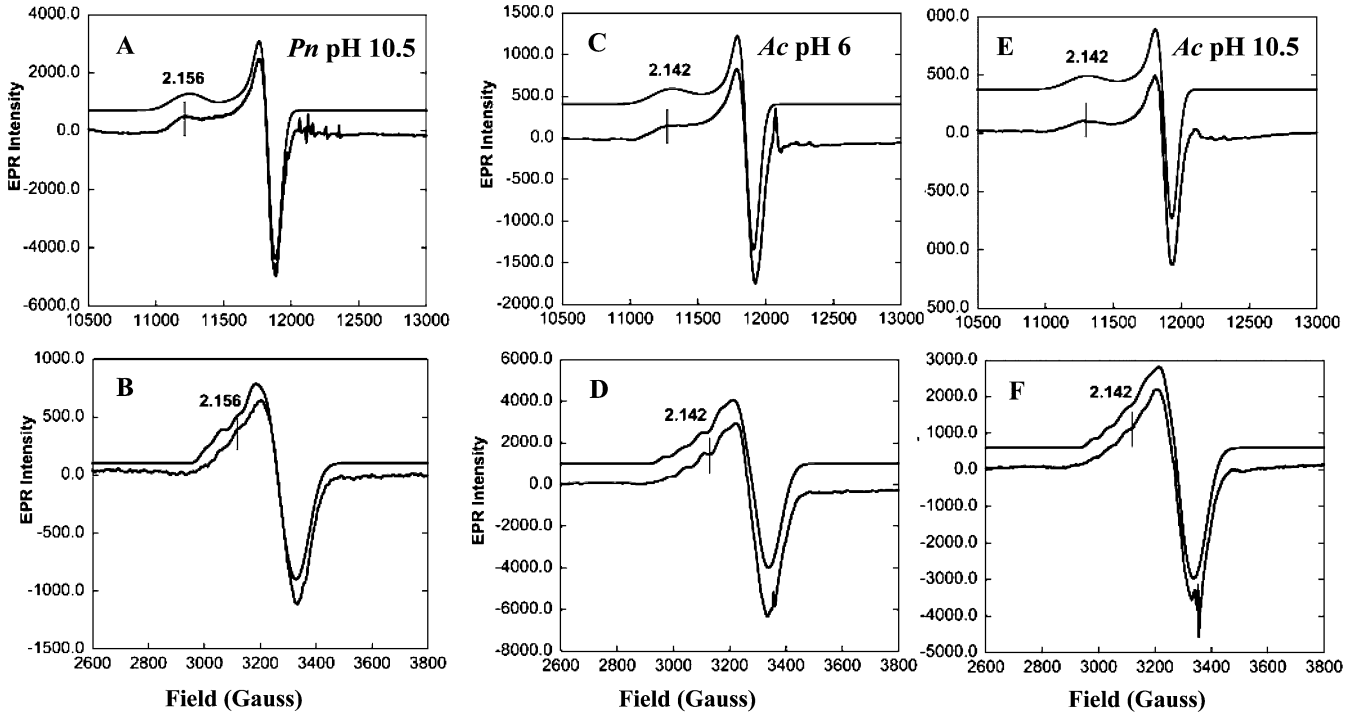

Figure 3. Experimental (lower) and simulated (upper) EPR spectra of Cu_Z: (A) Q-band, PnN_2OR, pH 10.5; (B) X-band, PnN_2OR, pH 10.5; (C) Q-band, AcN_2OR, pH 6; (D) X-band, AcN_2OR, pH 6; (E) Q-band, AcN_2OR, pH 10.5; (F) X-band, AcN_2OR, pH 10.5. EPR spectra were collected at 77 K, and 10mW power.

the negative pseudo-A signal (band 5) is more intense in AcN_2-OR than in PnN_2OR. Similar spectral differences can also be observed between the two enzymes at high pHs (Figure 2A,B,E,F). These reflect quantitative differences in S 3p contributions to the β-LUMO of the Cu_Z cluster in the two enzymes (see the Discussion section).

At high pH, the absorption and MCD spectra of PnN_2OR (Figure 2C,D) and AcN_2OR (Figure 2E,F) show intensities and energy positions of the bands similar to those in the spectra at low pH, with minor perturbations in the higher energy histidine-to-Cu CT region (band 9−13), indicating that the electronic structure of the Cu_Z cluster is not greatly perturbed on going from low to high pH for either enzyme.[49]

3.1.2. EPR. Figure 3 shows the Q- and X-band EPR spectra of dithionite-reduced (i.e., Cu_A reduced) samples of PnN_2OR (pH 10.5) and AcN_2OR (pH 6, 10.5). The g values of the enzymes have been extracted from Q-band EPR data, which give the $g_{||}$ value and show that the Cu_Z cluster has an axial EPR signal with $g_{||} > g_\perp > 2.003$, reflecting a $d_{x^2-y^2}$ ground state.

At pH 7, PnN_2OR has a $g_{||}$ value of 2.158 and a $g_\perp$ of 2.045 (Figure S5).[26] At pH 6, AcN_2OR has a $g_{||}$ value of 2.142 and a $g_\perp$ of 2.035 (Figure 3C,D, Table 2). Accurate g values obtained from Q-band EPR spectra were then correlated to the X-band spectra. The $g_{||}$ values of both PnN_2OR and AcN_2OR map onto a hyperfine feature. Since the electron spin coupling to one Cu would lead to a $g_{||}$ positioned between the $M_s = +^1/_2$ and $-^1/_2$ hyperfine lines, at least two Cu atoms were required to account for the metal hyperfine splitting in the X-band spectra of both PnN_2OR and AcN_2OR. The results of the simulations (Table 2) show that PnN_2OR has an $A_{||}$ of 61×10^{-4} cm^{-1} on one Cu and 23×10^{-4} cm^{-1} on the second Cu, indicating that the spin distribution on the two Cu atoms is in the ratio of 5:2, as published previously.[25] For AcN_2OR, $A_{||}$ values of 64×10^{-4} and 41×10^{-4} cm^{-1} were obtained, indicating that the unpaired electron is distributed over two Cu atoms in the ratio of ∼3:2. Simulation using three Cu atoms did not improve the goodness of fit.

Table 2. EPR Parameters of AcN_2OR and PnN_2OR at Low and High pHs, Simulated with Spin Densities Distributed on Two Cu Atoms

enzyme, pH	$g_{||}$	$g_\perp$	$A_{||}{}^a$	$A_\perp{}^a$	$A_{||}{}^a$	$A_\perp{}^a$
PnN_2OR, 7.0	2.158	2.045	61	25	23	20
PnN_2OR, 10.5	2.156	2.042	57	24	24	20
AcN_2OR, 6.0	2.142	2.035	64	22	41	20
AcN_2OR, 10.5	2.142	2.032	56	22	37	20

[a] All values $\times 10^{-4}$ cm^{-1}.

The EPR spectra of both PnN_2OR and AcN_2OR do not change significantly on increasing the pH to 10.5 (Figure 3). The $g_{||}$ values remain almost the same, while the $A_{||}$ values decrease by $(4-8) \times 10^{-4}$ cm^{-1} for the Cu atom, with dominant $A_{||}$ contribution (Table 2). This implies that the spin density (SD) distribution is only slightly perturbed by changing the pH. This will be addressed in section 3.2.

3.1.3. Resonance Raman. (a) Vibrations. The rR spectra of PnN_2OR excited at 600 nm and AcN_2OR excited at 620 nm at low and high pH in both ^{16}O and isotope-enriched ^{18}O (95−97%) buffers are presented in Figure 4. PnN_2OR at pH 7 has three dominant peaks at 366, 386, and 415 cm^{-1} (Figure 4A). Previous studies showed that these peaks shift to lower frequencies upon ^{34}S substitution.[20] On the basis of these isotope shifts, the vibrational frequencies, and the excitation profiles, these rR features have been assigned as Cu−S stretching

(49) In ref 26, a more significant change in MCD bands 4, 8, 9, and 10 was observed with increase in pH. However, this change appears to reflect a 10−15% contribution from oxidized Cu_A.

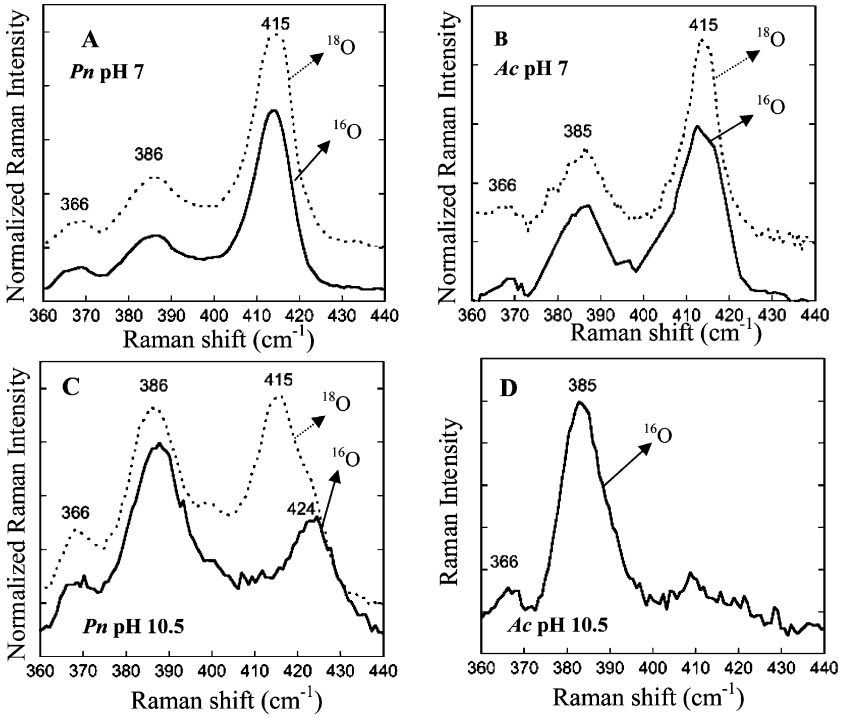

Figure 4. Resonance Raman spectrum of Cu_Z from (A) PnN_2OR at pH 7, excited at 600 nm (ref 26 showed PnN_2OR at pH 7 (^{16}O buffer), excited at 624.4 nm); (B) AcN_2OR at pH 7, excited at 620 nm; (C) PnN_2OR at pH 10.5, excited at 600 nm; and (D) AcN_2OR at pH 10.5, excited at 620 nm. Dotted lines present data in ^{18}O, and bold lines present data in ^{16}O buffer. All data were collected at 77 K. *Y*-axes in spectra A−C are normalized to the ^{18}O-independent 386 cm^{-1} (PnN_2OR) peak and the 385 cm^{-1} (AcN_2OR) peak. The ^{18}O data have been offset relative to the ^{16}O data. Note that data were not collected for ^{18}O samples of AcN_2OR at pH 10.5 since the 415 cm^{-1} or an equivalent mode was unobserved.

vibrations.[26] The ^{18}O samples of PnN_2OR at the same pH showed no measurable shift in the energy positions of the three peaks, consistent with the assignment of these modes as having dominantly Cu−S character.

AcN_2OR at pH 7 also has three similar features at 366, 385 and 415 cm^{-1} (Figure 4B), indicating a Cu_4S core similar to that of PnN_2OR. These three peaks also show no significant shift in their energy positions in ^{18}O buffer.

The rR spectra of the two enzymes at high pH (excited at 600 and 620 nm for PnN_2OR and AcN_2OR, respectively) are presented in Figure 4C,D. Importantly, in the case of PnN_2OR, the 415 cm^{-1} band disappears, and another peak with lower intensity is present at 424 cm^{-1} (Figure 4C). The rR profiles of the 415 cm^{-1} (low pH) and 424 cm^{-1} (high pH) vibrations are the same (*vide infra*), indicating that the corresponding vibrations are of similar origins. Thus, the 415 cm^{-1} peak at low pH shifts to 424 cm^{-1} at high pH. In the case of AcN_2OR, the peak at 415 cm^{-1} has lost essentially all of its intensity at high pH; however, no new rR vibration is observed (Figure 4D).

For PnN_2OR, ^{18}O data obtained at high pH show a significant 9 cm^{-1} shift of the 424cm^{-1} peak to 415 cm^{-1}. The calculated $^{18}O/^{16}O$ shift for a mode with pure oxygen motion at this frequency is 24 cm^{-1}. Thus, the 9 cm^{-1} $^{18}O/^{16}O$ shift indicates significant Cu−O character in the 424 cm^{-1} vibrational mode at high pH. At low pH there is no ^{18}O isotope shift; thus, this mode is mainly Cu−S in nature. The loss of rR enhancement of the 415 cm^{-1} mode in AcN_2OR at high pH (Figure 4D) may be a result of it having even higher Cu−O (relative to Cu−S) stretching character mixed in which would further decrease its resonance enhancement from a S−Cu CT transition.

(b) Profiles. The excitation profiles of the three dominant vibrations (366, 385/386, and 415 cm^{-1}) of both enzymes at low pH, overlaid with the absorption spectra with Gaussian fits (from absorption and MCD), are shown in Figure 5A,B. As reported earlier, for PnN_2OR, the 415 cm^{-1} mode mainly profiles band 7.[26] The 366 and 386 cm^{-1} vibrations are mainly resonance enhanced by bands 5 and 6 of the absorption spectrum (Figure 5A). As mentioned in section 3.1.1, the intensity patterns of the CT bands in the two enzymes are somewhat different. In the case of AcN_2OR, band 5 is the most intense, which is also reflected in the excitation profile (Figure 5B).

For AcN_2OR, the vibrations at 366 and 385 cm^{-1} profile mainly absorption band 5 and weakly band 6, and the 415 cm^{-1} vibration mainly profiles absorption bands 6 and 7. Since these vibrations are Cu−S stretches,[20] this supports the assignment of all three absorption bands as electronic transitions with substantial S−Cu CT character.

The rR profiles of the enzymes at high pH are presented in Figure 5C,D. For PnN_2OR, the rR profile at high pH is similar to that at low pH (Figure 5A,C), but with the 424 cm^{-1} band (at high pH) having the same profile as the 415 cm^{-1} at low pH. The intensity of the 424 cm^{-1} vibration is much weaker than that of the 415 cm^{-1} vibration at low pH. For AcN_2OR, at high pH, the vibrations at 366 and 385 cm^{-1} mainly profile absorption bands 5 and 6. The 385 cm^{-1} mode appears weakly enhanced by absorption band 7.

(c) pK_a. The pK_a values of the one-hole form ($1Cu^{II}/3Cu^{I}$) of PnN_2OR and AcN_2OR were determined by plotting the relative rR intensities of the 415 cm^{-1} peak (which decreased in intensity with increasing pH) and the 424 cm^{-1} peak (which increased in intensity with increasing pH) for PnN_2OR and the decreasing intensity of the 415 cm^{-1} peak for AcN_2OR with

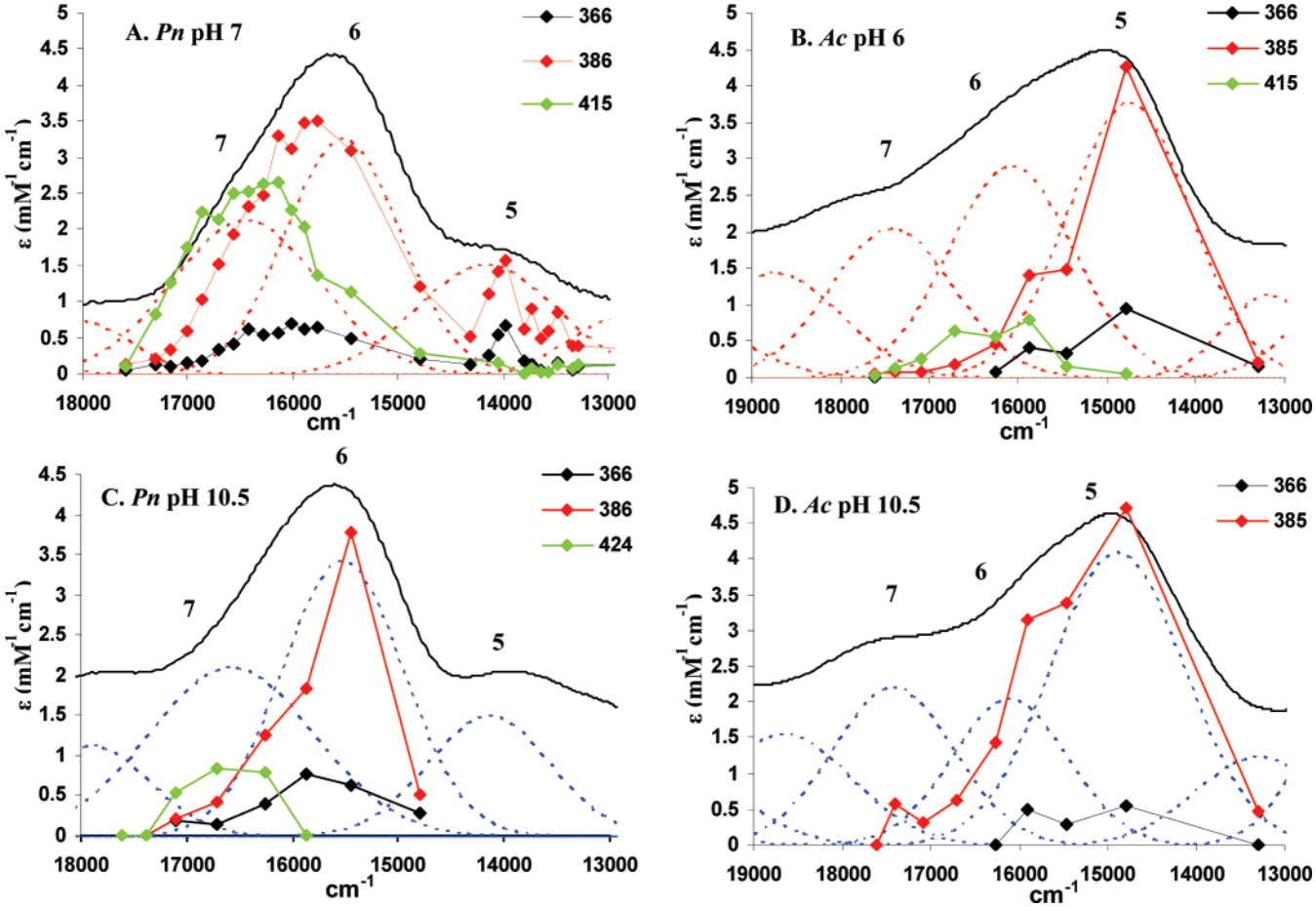

Figure 5. Cu_Z resonance Raman excitation profiles overlaid on the Cu_Z absorption spectrum (solid line) with Gaussian fits (dotted lines) and band numbers: (A) PnN_2OR, pH 7.0 (adapted from ref 26); (B) AcN_2OR, pH 6.0; (C) PnN_2OR, pH 10.5; and (D) AcN_2OR, pH 10.5.

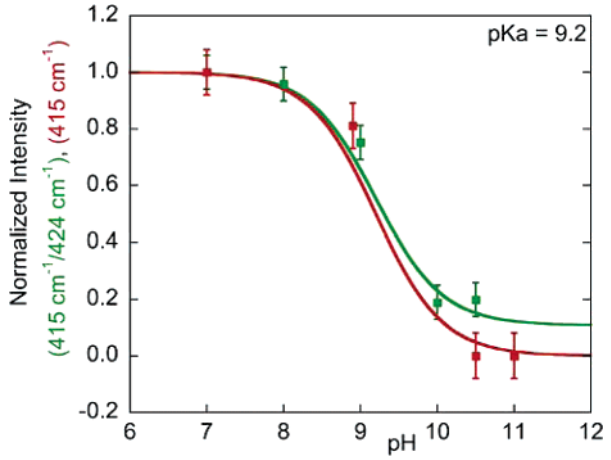

Figure 6. pK_a plots for PnN_2OR determined from the relative intensities of the 415 and 424 cm^{-1} peaks, excited at 600 nm (green), and AcN_2OR determined from the decrease in intensity of the 415 cm^{-1} peaks, excited at 620 nm (red).

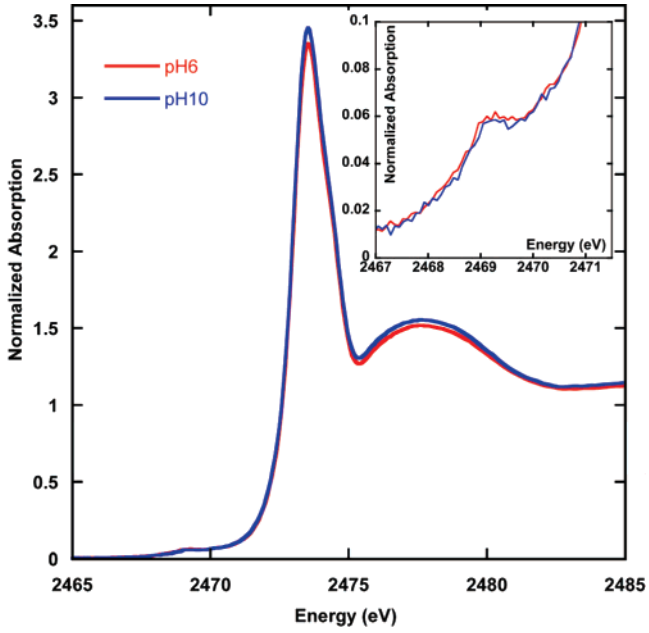

Figure 7. Normalized S K-edge spectra of AcN_2OR at pH 6 and 10,B $_B$and an expansion of the pre-edge region (inset). Note the weak pre-edge feature at ~2470 eV corresponds to the presence of a small amount of oxidized Cu_A.

increasing pH (it lacks the 424 cm^{-1} peak at high pH) over a pH range of 7−11 (Figure 6). The pK_a for both enzymes was found to be ~9.2 ($pK_a = 9.2 \pm 0.3$ for PnN_2OR and 9.2 ± 0.4 for AcN_2OR). The pH-dependent rR data for both enzymes are provided in Figure S3.

3.1.4. S K-Edges. Figure 7 shows a comparison of the normalized S K-edge spectra of AcN_2OR at pH 6.0 and 10. The spectra are essentially identical in both the rising edge region and the pre-edge region (expanded scale inset at 2469.2 eV). The energy of the pre-edge transition is very sensitive to the molecular environment of the μ_4-sulfide. The fact that the pre-edge does not change in intensity or energy between low

and high pH indicates that protonation of the bridging sulfide does not occur at low pH. Protonation would stabilize the 1s orbital of the μ_4-sulfide and shift the pre-edge transition (S 1s $\rightarrow$ β-LUMO), to higher energy. The similar pre-edge intensity at both pHs indicates that the Cu−S covalency is unchanged. However, the S contribution to the β-spin LUMO cannot be quantitatively determined from the pre-edge intensity due to the errors associated with the large renormalization factor (32 S atoms contribute to the edge transition, while only one, μ_4-S of Cu_Z, contributes to the pre-edge feature)[50] and the incomplete Cu and sulfide loading in the protein.

To summarize the experimental data, from rR spectroscopy, we observe that the 415 cm^{-1} vibration at low pH has dominant S character (from the ^{34}S isotope shift)[20] and no O character (lack of an ^{18}O isotope shift). Upon increasing the pH, this vibration shifts to higher energy, its resonance enhancement is decreased, and it now shows a 9 cm^{-1} ^{18}O isotope shift, indicating significant Cu−O stretching character. This strongly suggests the presence of a OH^- ligand in the Cu_ICu_{IV} edge of Cu_Z at high pH. From the absorption and MCD spectra of PnN_2-OR and AcN_2OR at both high and low pHs, there is no significant change in the ligand field (LF). The EPR data at high and low pHs indicate that the SD distribution remains unperturbed over the pH transition. These results argue against a significant change in the edge ligand with pH. The S K-edge XAS data have identical pre-edge energies and intensities between the high- and low-pH forms, suggesting that the μ_4-sulfide is not protonated in the one-hole form of the enzyme. Thus, we conclude that the μ_4-sulfide and OH^- edge ligands remain preserved at low pH. We suggest that a conserved lysine residue that is at H-bonding distance to the edge ligand (~3−4 Å) (Figure 1) is protonated with a pK_a of ~9.2, producing the observed pH effect. This is evaluated using DFT calculations below.

3.2. Computational Details. DFT calculations were used to obtain a detailed description of the $1Cu^{II}/3Cu^{I}$ state wave function (single unpaired electron, spin doublet) of the Cu_Z cluster of N_2OR in terms of how it is perturbed by different protonations. The geometric and electronic structures of the Cu_Z complexes with H_2O and OH^- (Figure 8) were evaluated to assess the influence of these ligands on the wave function and spectroscopic properties of the Cu_Z cluster. In the reported N_2-OR structures, the Cu_4S core of the Cu_Z center has approximate C_s symmetry, with the Cu_I-S-Cu_{II} angle (~160°) defining the mirror plane. The other Cu−S−Cu angles are close to 90°. The experimental Cu−S distances are in the 2.15−2.35 Å range, with the Cu_I−S bond being the longest.[3−7] These structural features of the Cu_Z cluster are reproduced in the DFT calculations (Table S1).

In the $[Cu_4S(im)_7(OH_2)]^{3+}$ species (Figures 8A and S1A), the water ligand is bound to only one copper atom, Cu_I.[32] The weak Cu_Z-OH_2 bond, with a distance of 2.23 Å and a bond order BO_{CuI-O} of 0.16, derives mostly from orbital interactions of the water ligand electron lone pair with the unoccupied Cu_I 4s orbital.[32] As a result, the α- and β-spin components of the bond order BO_{CuI-O} are equal (0.08, Table S2). If the lysine residue near the Cu_ICu_{IV} edge is absent or non-charged ($-NH_2$ tail group), the OH^- ligand occupies a bridging position between the Cu_I and Cu_{IV} atoms (Figures 8B,D and S1B,D). This bridging binding mode has been recently reported for a Cu_Z complex with iodide in the X-ray structure of AcN_2OR.[7] The bond orders BO_{CuI-O} and BO_{CuIV-O} are 0.56 and 0.38, respectively (Table S2), indicating a stronger covalent coupling between Cu_I and OH^-. The α- and β-spin components of the bond orders for the Cu_Z-OH^- interaction (Table S2) indicate that the OH^- ligand binding involves charge donation to Cu 4s,4p orbitals and, to a lesser degree, the unoccupied β-spin Cu 3d orbital. However, as shown below, H-bonding between the OH^- ligand and the protonated lysine residue can influence the binding position of the OH^- ligand at the Cu_ICu_{IV} edge.

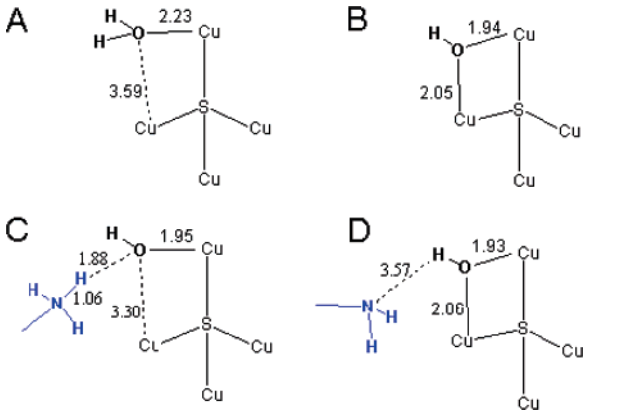

Figure 8. Optimized structures of (A) $[Cu_4S(im)_7(OH_2)]^{3+}$ and (B) $[Cu_4S(im)_7(OH)]^{2+}$ (adapted from ref 32) and (C) $[Cu_4S(im)_7(OH)]^{2+}$ with Lys and (D) $[Cu_4S(im)_7(OH)]^{2+}$ with $LysH^+$. See Figure S1 for complete structures.

Table 3. Atomic Spin Densities (NPA) of the Cu_Z Cluster for the Complexes with the Edge Ligand L and the $Cu-O_L$ Distances

	NPA atomic spin density (%)					$Cu-O_L$ distances (Å)	
species	Cu_I	Cu_{II}	Cu_{III}	Cu_{IV}	S	Cu_I-O	$Cu_{IV}-O$
$[Cu_4S(im)_7(OH_2)]^{3+}$ [a]	17.1	15.9	18.8	3.7	31.1	2.23	3.39
$[Cu_4S(im)_7(OH)]^{2+}$ [a]	31.5	5.9	4.1	10.1	29.9	1.94	2.05
$[Cu_4S(im)_7(OH)]^{2+}\cdots LysH^+$	44.9	6.3	3.2	3.6	21.3	1.95	3.30
$[Cu_4S(im)_7(OH)]^{2+}\cdots Lys$	33.6	6.4	3.4	9.2	30.4	1.93	2.05

[a] Adapted from ref 32.

The ground-state wave function and spin distribution in the Cu_Z cluster are influenced by the Cu_ICu_{IV} edge ligand (see below). In the Cu_Z cluster, Cu_I has the highest coordination number (CN) of 4, while the other Cu atoms have CNs of 2 and 3. In $[Cu_4S(im)_7(OH)]^{2+}$, the valence indices[46] (Table S1) of the copper atoms are 2.20 (Cu_I), 1.96 (Cu_{II}), 1.90 (Cu_{III}), and 1.87 (Cu_{IV}). Since Cu_I has a stronger LF, as reflected by its atomic valence, it carries a higher charge, and the unpaired electron is mostly localized on this copper atom (31.5%, Table 3).

In $[Cu_4S(im)_7(OH_2)]^{3+}$, the valence indices (Table S1) of the copper atoms are 1.96 (Cu_I), 2.12 (Cu_{II}), 2.26 (Cu_{III}), and 1.85 (Cu_{IV}). Since Cu_{IV} has the weakest LF, it carries only less than 4% SD, and Cu_I, Cu_{II}, and Cu_{III} have SDs of 16−19% each. Thus, the conversion from L = H_2O to L = OH^- should cause a noticeable change of the SD of the cluster (Table 3), which is not observed experimentally (Section 3.1). Such a change in the ground-state wave function should also cause a substantial change in the absorption spectrum of the Cu_Z cluster, especially

(50) The edge in a S K-edge spectrum is a result of all S 1s $\rightarrow$ 4p transitions; however, the pre-edge feature is a S 1s $\rightarrow$ β-LUMO transition, and its intensity is proportional to the % orbital character of the μ_4-sulfide of Cu_Z in the mostly Cu 3d-based β-LUMO. Non-coordinated S cannot contribute intensity to the pre-edge.

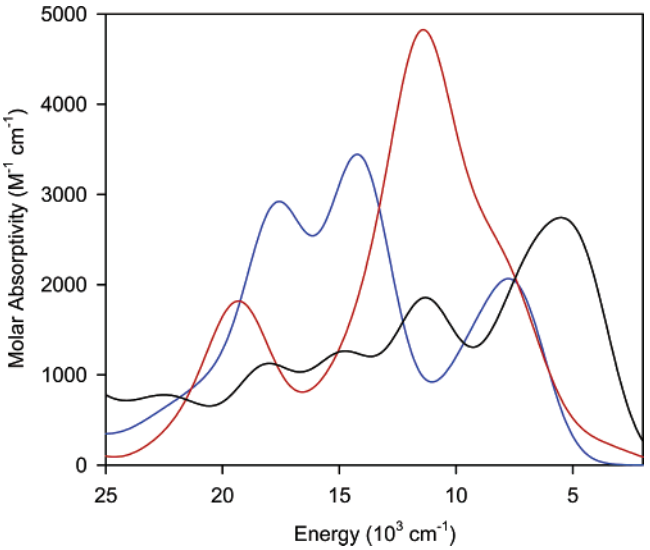

Figure 9. TD-DFT calculated absorption spectra of $[Cu_4S(im)_7(OH_2)]^{3+}$ (blue line), $[Cu_4S(im)_7(OH)]^{2+}$ (red line), and $[Cu_4SH(im)_7(OH_2)]^{4+}$ (black line).

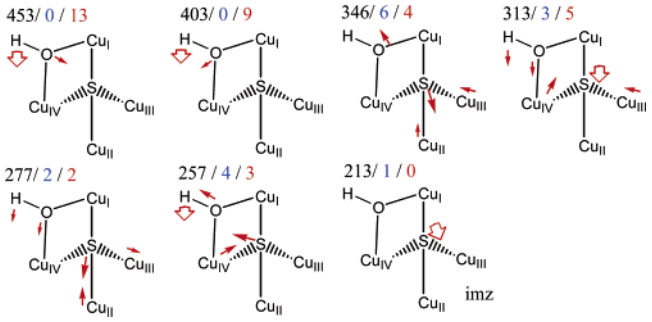

Figure 10. Calculated Cu−S and Cu−OH normal modes of $[Cu_4S(im)_7(OH)]^{2+}$. The arrows indicate atomic displacements, and band frequencies (cm^{-1}) and ^{34}S and ^{18}O isotope shifts (cm^{-1}) are shown in black, blue, and red, respectively. The Cu−S and Cu−O bond length distortions for these bands are given in Table S3. The bands with significant imidazole displacement contributions are indicated by "imz".

in LF transitions, as observed in the TD-DFT-calculated absorption spectra of $[Cu_4S(im)_7(OH_2)]^{3+}$ and $[Cu_4S(im)_7(OH)]^{2+}$ (Figure 9). However, the absorption features of Cu_Z in the protein at low and high pH are very similar (Figures 2 and S4). This observation argues that the protonation process with a pK_a of 9.2 is not associated with the transformation of the edge ligand between H_2O and OH^-. Since the rR data provide strong evidence of OH^- binding to the Cu_Z cluster at high pH, the small changes in the absorption and EPR features of the Cu_Z cluster indicate that the OH^- ligand at the Cu_ICu_{IV} edge remains preserved at low pH.

Harmonic frequency calculations were performed to estimate vibrational frequencies of the Cu_Z species $[Cu_4S(im)_7(OH)]^{2+}$ and evaluate ^{34}S and ^{18}O isotope shifts of vibrational bands. The calculated data for the Cu_Z cluster are summarized in Figure 10. The vibrational modes of the Cu_4S cluster involve four Cu−S-based stretching modes: two in-plane modes from Cu_I−S/Cu_{II}−S vibrations (both symmetric, assuming C_s symmetry for the Cu_4S cluster) and two out-of-plane modes, one a symmetric combination of the Cu_{III}−S/Cu_{IV}−S stretches and the other the antisymmetric combination of the Cu_{III}−S/Cu_{IV}−S stretches. Given the low symmetry of the Cu_4S cluster, this normal mode classification becomes somewhat approximate but still remains helpful. The Cu−S vibrational bands occur at 360−440 cm^{-1} (Figure 4) and shift to lower frequencies upon ^{34}S isotope labeling.[20] However, they can kinematically couple with other metal−ligand vibrational bands such as Cu−imidazole and Cu−L (L = edge ligand) bands (Table S3) because the latter are also present in the low-frequency region of the vibrational spectrum and have force constants similar to those for the Cu−S stretching bands. The kinematic coupling between the Cu−S and Cu−OH^- bands for the $[Cu_4S(im)_7(OH)]^{2+}$ complex (Figure 10) is strong, and the corresponding vibrations exhibit pronounced ^{34}S and ^{18}O isotope shifts. This is consistent with the experimental data (section 3.1) that indicate that, at high pH, the rR bands with mostly Cu−S character show a 9 cm^{-1} ^{18}O isotope shift for the 424 cm^{-1} band of PnN_2OR. Note that, if the OH^- is replaced by H_2O, the Cu−OH_2 frequency is greatly lowered and does not mix with the Cu−S core vibrations (Table S4).

In the rR spectra of N_2ORs at low pH, three vibrational bands with significant Cu−S character have been identified at 366, 385/386, and 415 cm^{-1}, with ^{34}S isotope shifts of −2, −6, and −7 cm^{-1}, respectively, [20] and no detectable ^{18}O isotope shifts. This indicates that, in going from high pH to low pH, the position of the OH^- ligand of the Cu_Z cluster is perturbed and the kinematic coupling between the Cu−S and Cu−OH^- bands is disrupted. Such a change can be caused by the strong noncovalent interaction between the OH^- ligand and the protonated lysine residue nearby. When the lysine residue is protonated, the proton of the $-NH_3^+$ tail of the lysine functions as an H-bond donor to the OH^- ligand (the N_{lys}−O_{OH} distance is 2.90 Å), causing the ligand to move away from the Cu_{IV} atom ($\Delta d_{Cu_{IV}-O} = +1.25$ Å) and closer to the lysine $-NH_3^+$ group (Table 3, Figures 8C and S1C). However, since the SD on the Cu_{IV} atom in $[Cu_4S(im)_7(OH)]^{2+}$ is only 10% (Table 3), this change in the OH^- ligand position does not significantly perturb the ground-state wave function. Consequently, the SD distribution in the Cu_Z cluster remains similar to that when the OH^- ligand occupied the bridging position at the Cu_ICu_{IV} edge (Table 3).

We also applied TD-DFT to probe the effect of possible protonation of the μ_4-S ion on the absorption spectrum of the Cu_Z cluster at low pH (the $[Cu_4SH(im)_7(OH_2)]^{4+}$ species, Figure 9; geometry-optimized structure in Figure S6),[51] as has been considered in ref 28. The calculated spectrum is very different from the spectra of the non-protonated Cu_Z species (Figure 9). The most pronounced spectral charge is the disappearance of the strong CT bands near 15 600 cm^{-1} due to the stabilization of the μ_4-S occupied orbitals and the significant blue shift of the corresponding S−Cu CT excitations. This is not observed experimentally. Combined with the fact that there is no change in the S K-edge spectrum of the protein at low pH (section 3.1.4), this provides strong evidence that the small spectral changes observed upon pH variation in N_2ORs do not involve protonation of the μ_4-sulfide of the Cu_Z cluster.

3.3. Kinetics. The rate of reduction of the resting one-hole ($1Cu^{II}/3Cu^{I}$) form of PnN_2OR to the fully reduced active form in the presence of 500-fold excess of reduced MV was measured at different pHs (Figure 11). The amount of one-hole Cu_Z was

(51) Protonation of the μ_4-S ion of Cu_Z is less favorable in energy relative to protonation of the OH^- edge ligand by ~108 kcal mol^{-1} (ΔE_{el} at the B3LYP level, in vacuum).

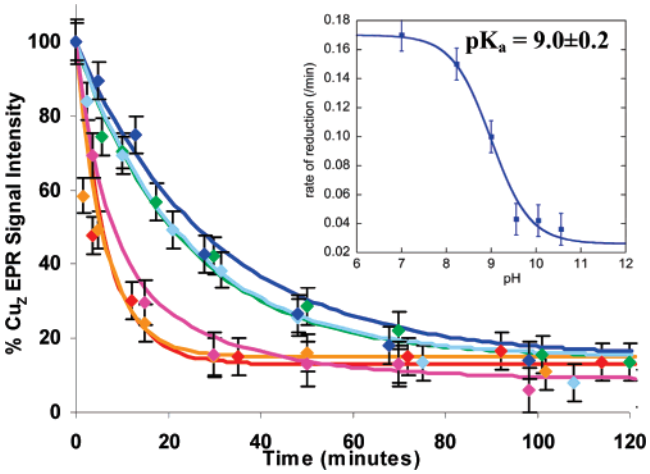

Figure 11. Rates of reduction of PnN_2OR at different pHs (red, pH 7.0; orange, pH 8.2; pink, pH 9.0; green, pH 9.5; light blue, pH 10.0; blue, pH 10.5). Inset: Determination of $pK_a = 9.0 \pm 0.2$.

determined from the intensity of the Cu_Z EPR signal. The rate of reduction decreased with increase in pH. The rates have been simulated using a single-exponential decay, which gives a low-pH-limit rate constant as 0.18 min^{-1} (pH 7) and a high-pH-limit rate constant as 0.034 min^{-1} (pH 10.5).[52] Thus, the rates of reduction differ by a factor of 5−6 on going from low to high pH, with a pK_a of ∼9.0 ± 0.2 (Figure 11, inset).

4. Discussion

A combination of various spectroscopic techniques and DFT calculations has provided insight into the effect of pH on the geometric and electronic structure of the resting one-hole form of the Cu_Z clusters in PnN_2OR and AcN_2OR and the possible contribution of protonation to the rate-determining step in turnover.

4.1. pH Effect. There is no observed change in the pre-edge energy and intensity of the S K-edge spectra of the one-hole form of AcN_2OR at low and high pHs, implying that there is no protonation of the bridging μ_4-sulfide at low pH. The TD-DFT-calculated spectrum of the μ_4-sulfide form is in good agreement with the experimental absorption spectrum. However, it is significantly different from the spectrum of the μ_4-SH^- form, $[Cu_4SH(im)_7(OH_2)]^{4+}$. These results eliminate the possibility of a μ_4-sulfide protonation of the Cu_Z cluster at low pH.

The rR data of PnN_2OR at high pH show that the 415 cm^{-1} Cu−S stretching vibration shifts to higher frequency, loses intensity, and now shows a 9 cm^{-1} ^{18}O shift, while the 415 cm^{-1} band in AcN_2OR loses all intensity at high pH. This implies significant Cu−O stretching character mixed into this high-frequency mode, indicating the presence of a OH^- ligand bound at the edge. These experimental results at high pH are also supported by DFT calculations, which show that the kinematic coupling between the Cu−S and Cu−OH^- modes for the $[Cu_4S(im)_7(OH)]^{2+}$ complex is strong, resulting in pronounced ^{34}S and ^{18}O isotope shifts of the vibrational frequencies. In contrast, the absorption, MCD, and EPR spectra of the enzymes at both low and high pH do not detect significant perturbations of the ground-state wave function. DFT-calculated

(52) The data at pH 9 have been simulated using a double-exponential expression, taking into account the different rates of reduction of the low-pH form and the high-pH form.

Scheme 1. pH Effect in (A) PnN_2OR and (B) AcN_2OR

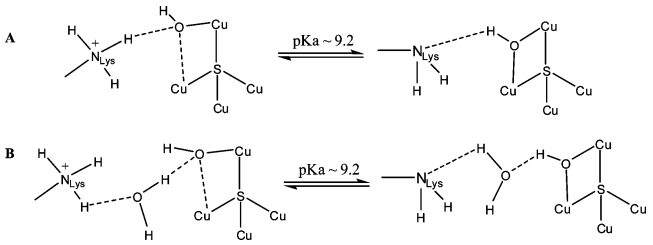

spin densities and the TD-DFT-calculated absorption spectra of the enzyme with H_2O as the edge ligand are very different than the spectra of the enzyme with OH^- as the edge ligand, implying that the Cu_ICu_{IV} edge ligand remains OH^- in the low-pH region.

The rR spectrum at low pH is significantly different from the high pH rR spectrum. The 415 cm^{-1} vibration in the low-pH form has dominant Cu−S character (from its ^{34}S isotope shift)[20] and no Cu−O character (lack of an ^{18}O isotope shift), reflecting that the Cu−S vibration coupling to the OH^- ligand is perturbed in the pH transition. We propose that a highly conserved lysine residue, which is at H-bonding distance from the edge ligand, is protonated at physiological pH (pK_a of ∼9.2), which results in a change in the position of the OH^- ligand. DFT calculations, which include the lysine residue near the Cu_I-Cu_{IV} edge, support this model, since the calculations yield a similar SD distribution for the Cu_Z cluster (as observed in absorption, MCD, and EPR data) but different orientations of the OH^- ligand (which would lead to a different vibrational coupling in the rR spectrum) between protonated and deprotonated lysine forms (Figure 8C,D). Thus, the observed pH-dependent spectroscopic changes are most reasonably assigned to a protonation of the lysine residue near the Cu_ICu_{IV} edge of the Cu_Z cluster, leading to its H-bonding to the OH^- ligand of Cu_Z (Scheme 1A).

4.2. Differences in the Protein Sites of PnN_2OR and AcN_2OR. There are some resolvable spectral differences between PnN_2OR and AcN_2OR. The $g_{||}$ and $g_\perp$ values of AcN_2-OR are smaller than those of PnN_2OR (Table 2), and the unpaired electron is more delocalized in Cu_Z of AcN_2OR (the spin distribution over two Cu atoms is 3:2, compared to 5:2 for PnN_2OR from EPR spectroscopy). All the CT and LF bands are blue-shifted in AcN_2OR. Also band 5 in AcN_2OR gains intensity, as reflected in its absorption, MCD, and rR profile data, compared to that in PnN_2OR. Interestingly, the IT band (band 2, Figure 2) in PnN_2OR is more intense than that in AcN_2-OR. These differences between the two enzymes are consistent with the presence of an additional or more strongly bound edge ligand in AcN_2OR, as is reported in its crystal structure (Figure 1B).[7] An additional/stronger ligand near Cu_{IV} would increase the SD on Cu_{IV} (due to the stronger LF) and lead to enhanced S p_z' (oriented along the $Cu_{III}Cu_{IV}$ vector, Figure S2) mixing into the β-LUMO, which would be consistent with the enhanced intensity of band 5 (electron excitation from the occupied MO with the S p_z' character to the β-LUMO, Table 1) in AcN_2OR. The IT transition reflects the coupling and electron delocalization between Cu_I and Cu_{II}, mediated by the bridging sulfide via the Cu_I-S-Cu_{II} $\sigma-\sigma$ superexchange pathway.[26] A higher SD on Cu_{IV} would lead to a lower SD on Cu_{II} and thus a lower intensity of the IT band in AcN_2OR. An additional or more strongly

Scheme 2. Reaction Mechanism for N_2O Reduction by the Cu_Z Cluster (energies in kcal mol^{-1})

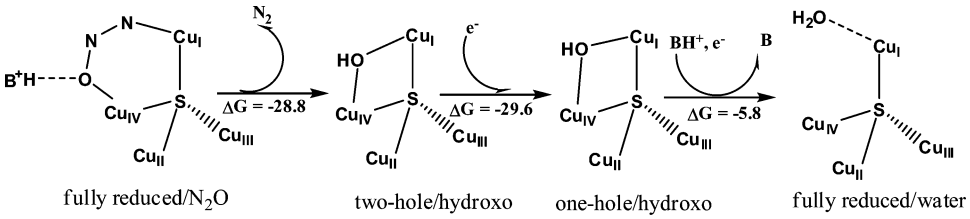

bound edge ligand would also lead to an increased LF in AcN_2-OR, as is reflected in the blue-shifted transition energies and the lower EPR g value.

4.3. Relevance to Reactivity. Our past studies indicate that the one-hole ($1Cu^{II}/3Cu^{I}$) form of the Cu_Z cluster must be reduced to the $4Cu^{I}$ form to be catalytically active.[30,31] The slow rate of reduction of the resting Cu_Z center (0.18 min^{-1} at pH 7) is much slower than the turnover rate ($\sim 10^3$ sec^{-1} for PnN_2OR at optimum pH of $\sim$8). However, it is important to note that the reducing agent, MV, is not the physiological reductant of the enzyme. The experimental rate of reduction decreases by a factor of 5−6 with increase in pH, with a pK_a of 9.0 ± 0.2 (Figure 11), which is close to the pK_a we suggest to be associated with the lysine residue near the Cu_ICu_{IV} binding site. The protonated form of lysine can tune the redox potential of Cu_Z, making it more positive, and accelerate the reduction rate of the Cu_Z cluster.

In ref 32, we have calculated that the barrier ($\Delta G^{\ddagger}$) for the direct cleavage of the N−O bond for $[Cu_4S(im)_7N_2O]^{2+}$ is 18 kcal mol^{-1}. In the transition state, an electron is transferred from the Cu_Z cluster to N_2O, activating the oxygen atom of the N_2O ligand for protonation. The protonated lysine residue near the edge could further lower this activation barrier. Computationally, the barrier for N−O bond cleavage decreases to 9 kcal mol^{-1} with an acidic H-bond donor. The calculated free energy for the protonated cleavage product in the reaction mechanism generating $[Cu_4S(im)_7(OH)]^{3+}$ with $2Cu^{II}$ is −28.8 kcal mol^{-1} (Scheme 2).[32] The reduction of the hydroxo species is energetically favorable ($\Delta G = -29.6$ kcal mol^{-1} for an e^- from Cu_A), generating the corresponding one-hole hydroxo form, $[Cu_4S(im)_7(OH)]^{2+}$. The proton-coupled reduction of this form to the fully reduced form can be lowered by protonation of the lysine residue at low pH. The calculated free energy for this step is −5.8 kcal mol^{-1} (Scheme 2).

5. Summary

We have determined that the Cu_ICu_{IV} edge ligand of the one-hole state of N_2OR is OH^- in both the low-pH (active) and high-pH (inactive) forms. Also, the μ_4-sulfide of Cu_Z remains deprotonated at low pH. The observed pH effect likely reflects a neighboring lysine residue, which can H-bond with the edge ligand at low pH. The protonated form of this lysine can increase the redox potential of Cu_Z and provide a proton to lower the barrier of the N−O bond cleavage and drive the reduction of the one-hole Cu_Z to the catalytically active fully reduced form in the reaction cycle.

Acknowledgment. This research was supported by NIH Grant DK-31450 (E.I.S.), POCTI/BME/42265/2001 (I.M.), and MCB-0347871 (D.M.D). S.I.G. is grateful to NSERC (Ottawa) for a postdoctoral fellowship. SSRL operations are funded by the U.S. Department of Energy, Office of Basic Energy Sciences. The Structural Molecular Biology program is supported by the National Institutes of Health, National Center for Research Resources, Biomedical Technology Program, and by the U.S. Department of Energy, Office of Biological and Environmental Research.

Supporting Information Available: DFT-optimized structures with different edge ligands and second-sphere amino acid residues; the Cu_Z structure with coordinate systems; rR data at different pHs; absorption, MCD, and EPR data on PnN_2OR, pH 7; DFT-optimized structure of sulfide-protonated Cu_Z cluster; complete ref 38; and tables with bond lengths and orders, atomic valence indices, and bond distance distortions for normal modes. This material is available free of charge via the Internet at http://pubs.acs.org.

JA068059E